Chapter 1

General Introduction

1.1 Introduction

The term perovskite describes a family of materials that have a structure similar to that of the mineral $CaTiO_3$[1]. Compounds with the perovskite structure have been widely studied since the 1940's, primarily because of the physical and electronic properties materials with this structure possess. Perovskites with useful properties such as ferroelectricity and piezoelectricity, including barium titanate and lead zirconium titanate, are the backbone of the electroceramic industries, which were estimated to be worth $15-20 billion a year at the turn of the century[1-3]. Perovskite-type materials also exhibit other properties, such as ferromagnetism, colossal magneto-resistance, super-conductivity and ionic conductivity, that are of significant technological and academic interest[1]. In the last 50 years many double perovskites have also been synthesised and studied for potential application. The existence of a large number of compounds with this structure leads to members of the double perovskite family exhibiting a wide range of fascinating properties[1, 2].

The interesting properties of perovskites are known to be strongly linked to subtle structural variations. A good example of this is that varying the degree of octahedral tilting in a perovskite changes the extent of orbital overlap through the BO_6 octahedral network thereby affecting electronic properties such as conductivity, magnetism and certain dielectric properties[4]. Therefore control of the degree of tilting in the perovskite structure can be used to optimise these properties. Despite this, until the 1980's the structures of perovskite-type materials were not well characterised[2]. In many cases perovskite samples have only been successfully synthesised in polycrystalline form and until recently the availability of synchrotron X-ray and neutron diffractometers, which are required in order to obtain precise and accurate structural information about complex polycrystalline samples, has been scarce. As a result of the link between the structure and properties of these compounds it is expected that further understanding of the factors responsible for stabilising the various perovskite structures will play a crucial role in designing materials with

improved properties. In particular there is significant interest in understanding the structure and properties of perovskites containing oxygen vacancies and/or cations with mixed valencies. This stems from the interest in the use of such materials for their ionic and electronic conducting properties in applications such as solid oxide fuel cells (SOFCs) and oxygen sensors[1, 5]. Mixed valence cations and oxygen vacancies are known to be related to electronic and ionic conductivity, so understanding the relative stability of these in the perovskite structure is important.

The work presented in this thesis describes the structures of double perovskites of the type $Ba_2LnB'O_{6-\delta}$ (Ln = lanthanide or Y^{3+} and B' = Nb^{5+}, Ta^{5+}, Sb^{5+} and/or Sn^{4+}). The aim of this work was to develop greater understanding of the structure of double perovskites, and in particular to establish why different variants of the double perovskite structure are adopted. In the case of the Sn^{4+} containing perovskites investigation of the structures with oxygen vacancies and lanthanides with mixed valencies has been undertaken. Of particular interest was the study of potential ordering of oxygen vacancies in the structure and the relative stability of oxygen vacancies compared to valence transitions of the lanthanide cations.

1.2 The Perovskite Structure

The first step in an examination of changes in the double perovskite structure is to examine the basic perovskite structure and the ways in that it can distort. The most sensible place to begin such an examination is the basic ternary perovskite structure, of which the double perovskite represents an ordered variant. The ideal ternary perovskite has the formula ABX_3 where the A-site cations are usually bigger than the B-site cations and X represents any anion. While perovskite compounds are known to contain a wide variety of anions, oxides are the most common. In perovskite-type oxides the A-cations are surrounded by twelve oxygen anions in a cubo-octahedral arrangement and occupy the space between the corner sharing BO_6 octahedra (see Figures 1.1 and 1.2). The symmetry of this ideal perovskite is $Pm\bar{3}m$ with $SrTiO_3$ being the archetype perovskite of this type. This structure is very demanding with the *a* lattice parameter being the only variable. Consequently the majority of perovskites vary from this structure in one of, or a combination of, three ways; octahedral tilting,

distortions in the length of the BO_6 octahedral bonds and B-cations displacements within the octahedra (see Figure 1.2)[1, 6]. All of these distortions occur to achieve the best possible compromise between the bonding requirements of the A- and B-site cations and thereby attain the structure with the lowest possible energy. These distortions lead to the formation of phases with lower symmetry.

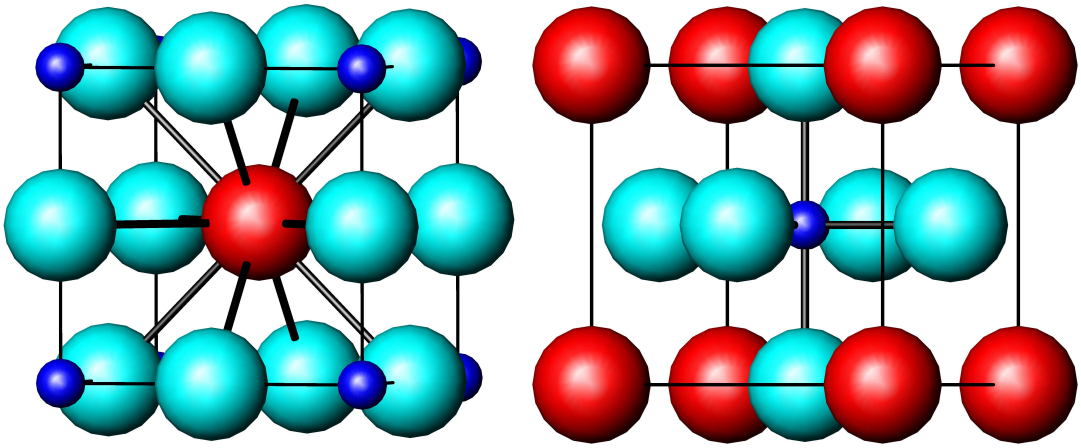

Figure 1.1: Two depictions of the unit cell of the ideal cubic perovskite structure highlighting the A-site cation environment (left) and the B-site cation environment (right). The red, dark blue and light blue spheres represent the A-site, B-site and oxygen anions respectively.

The suitability of a particular combination of cations for the perovskite structure can be estimated by the use of the tolerance factor *t* (see Equation 1.1) where r_A = radius of the A-site cation, r_B = radius of the B-site cation and r_O = radius of O^{2-}.

$$t = \frac{(r_A + r_O)}{\sqrt{2}(r_{(B)} + r_O)} \qquad \textbf{1.1}$$

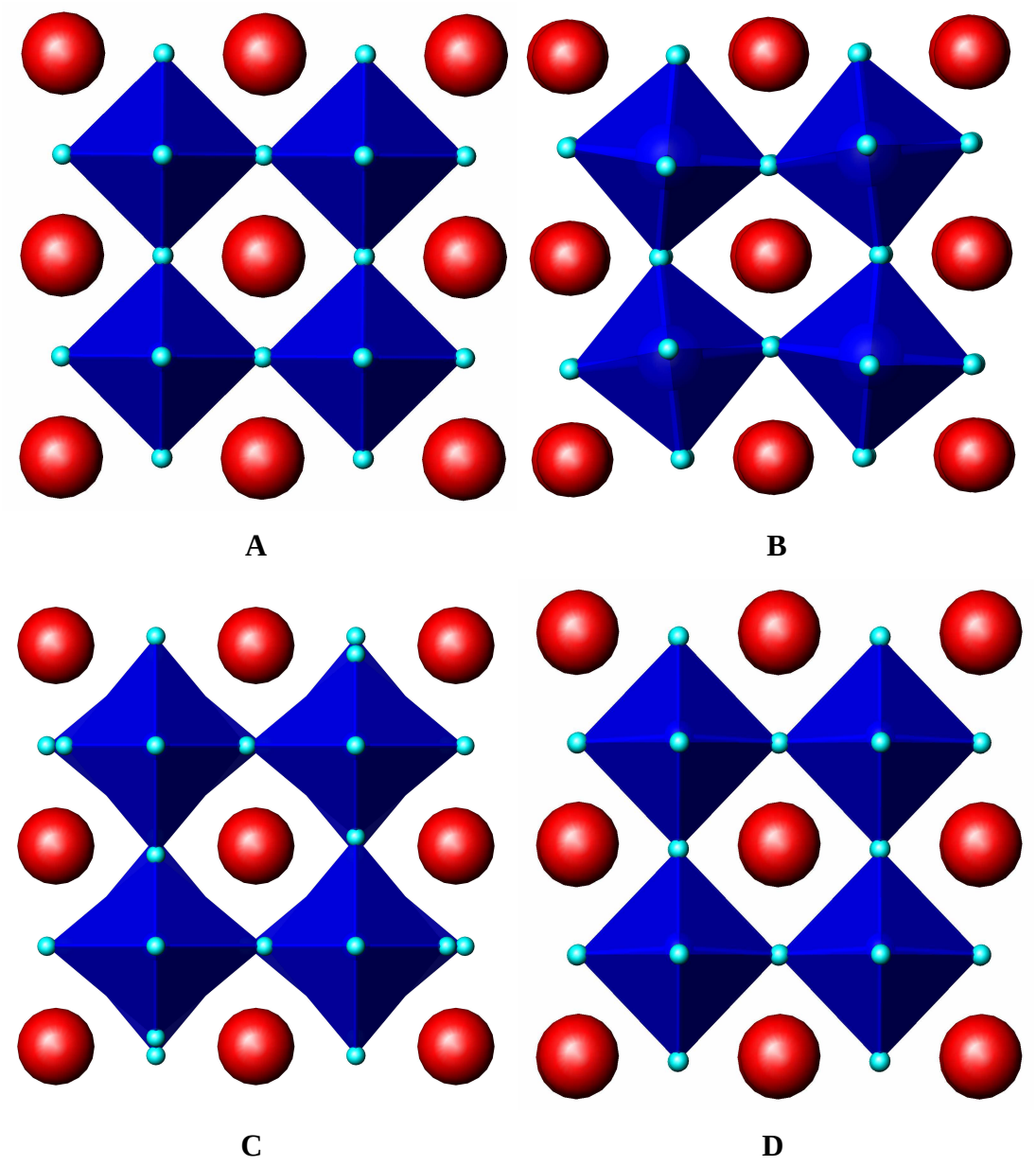

Figure 1.2: Depictions of the ideal perovskite and the three common types of distortion. The diagrams are of the ideal perovskite (**A**), an octahedral tilted perovskite (**B**), a perovskite with distortions in the BO_6 bonds (**C**) and a perovskite with the B-site cations displaced from the centre of the octahedra (**D**). The blue octahedra represent the BO_6 octahedra and the red spheres indicate the A-type cation.

The tolerance factor was first derived by Goldschmidt[7] over 80 years ago by treating the lattice as a close-packed array of hard spheres. The ideal size combination (i.e. $t = 1$) of the A- and B-site cations requires the B-O bond distance to be a factor of $\sqrt{2}$ less than the A-O bond distance. A tolerance factor of less than one indicates that the A-site cation is too small, compared to the B-site cation, and vice versa. In general the

more *t* deviates from 1 the more distorted from the ideal cubic perovskite the structure tends to be. Octahedral tilting is the most common of these possible distortions and occurs as a result of the A-site cation being too small for the 12-fold site within the BO_6 octahedral framework[1]. To accommodate this, the BO_6 octahedra tilt about the pseudo-cubic axes while retaining corner connectivity. In the majority of cases the tilting is near rigid, such that the bonds in the BO_6 octahedra remain approximately equal. Tilting results, however, in changing the 12 A-site co-ordination environment such that the 12 A-O bond lengths are no longer required to be equal.

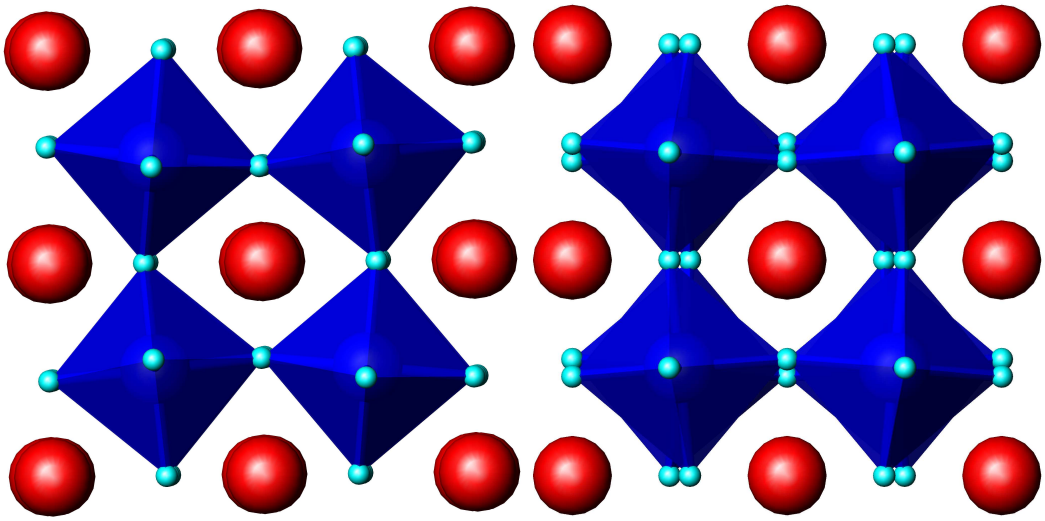

Figure 1.3: Crystal structure of *Cmcm* (tilt system $a^0b^+c^-$) viewed along the *b*-(left) and *c*-axis (right) highlighting the in- and out-of-phase tilting present in the structure.

The notation most commonly used to describe the octahedral tilting in perovskites is that developed by Glazer[8]. This notation describes the octahedral tilting around the three orthogonal axes of the cubic archetype. In the case of unequal tilting around each of these axes the rotation is described as $a^{\pm}b^{\pm}c^{\pm}$. The superscript refers to either in-phase tilting (+) where octahedra in alternating layers rotate in the same sense or out-of-phase tilting (-) where octahedra in alternating layers rotate in alternating directions (see Figure 1.3). Where the tilting around two or more of these axes is equal the letter used to describe the tilting is the same. An example of this notation is the orthorhombic *Pnma* structure, adopted by $GdFeO_3$, which is notated $a^-b^+a^-$ indicating the octahedra tilts around the *b*-axis are in-phase with each other and those around the pseudo-cubic *a*- and *c*-axis have equal magnitude and occur in an out-of-

phase fashion. Glazer originally suggested there are 23 possible tilt systems that leave the corner-sharing of the octahedra structures intact[8]. It should be noted that rearrangement of the type of octahedral tilting around each crystallographic axis, as a result of employing a different setting of the same space group, is common. An example of this is *Pnma* ($a^-b^+a^-$) and *Pbnm* ($a^-a^-c^+$) which are different arrangements of the same tilt system.

Table 1.1: Unit cell descriptions and atomic positions for all the space groups generated by tilting of the BO_6 octahedra of the primitive cubic structure. In general these are for the settings of the space groups employed in the group theoretical analysis of Howard and Stokes[9]. For tilt systems $a^0b^-b^-$ and $a^+b^-b^-$ two alternate commonly used space groups are given and for $a^-b^-c^-$ and $a^-a^-c^-$ the more commonly used $I\bar{1}$ and *I*2/*a* settings are described. a_p is the unit cell length of the primitive cubic structure and the tilt system given is specific to the crystallographic setting detailed.

Space Group (Tilt System)	Unit-cell Size	Atomic Positions (Wyckoff Symbol, Co-ordinates)		
		A	B	O
$Pm\bar{3}m$ ($a^0a^0a^0$)	$a = b = c = a_p$	1*b* (½,½,½)	1*a* (0,0,0)	3*d* (½,0,0)
*P*4/*mbm* ($a^0a^0c^+$)	$a = b \approx \sqrt{2}a_p$ $c \approx a_p$	2*c* (0,½,½)	2*a* (0,0,0)	2*b* (0,0,½) 4*g* (x,x+½,0) x ≈ ¼
*I*4/*mmm* ($a^0b^+b^+$)	$a \approx 2a_p$ $b = c \approx 2a_p$	2*a* (0,0,0) 2*b* (0,0,½) 4*c* (½,0,0)	8*f* (¼,¼,¼)	8*h* (x,x,0) x ≈ ¼ 16*n* (0,y,z) y ≈ ¼, z ≈ ¼
$Im\bar{3}$ ($a^+a^+a^+$)	$a = b = c \approx 2a_p$	2*a* (0,0,0) 6*b* (0,½,½)	8*c* (¼,¼,¼)	24*g* (0,y,z) y ≈ ¼, z ≈ ¼
Immm ($a^+b^+c^+$)	$a \approx 2a_p$ $b \approx 2a_p$ $c \approx 2a_p$	2*a* (0,0,0) 2*b* (0,½,½) 2*c* (½,½,0) 2*d* (½,0,½)	8*k* (¼,¼,¼)	8*l* (0,y,z) y ≈ ¼, z ≈ ¼ 8*m* (x,0,z) x ≈ ¼, z ≈ ¼ 8*n* (x,y,0) x ≈ ¼, y ≈ ¼
*I*4/*mcm* ($a^0a^0c^-$)	$a = b \approx \sqrt{2}a_p$ $c \approx 2a_p$	4*b* (½,0,¼)	4*c* (0,0,0)	4*a* (0,0,¼) 8*h* (x,x+½,0) x ≈ ¼
Imma ($a^0b^-b^-$)	$a \approx 2a_p$ $b \approx \sqrt{2}a_p$ $c \approx \sqrt{2}a_p$	4*e* (0,¼,z) z ≈ ¾	4*b* (¼,¼,¼)	4*e* (0,¼,z) z ≈ ¼ 8*g* (x,0,0) x ≈ ¼
Ibmm ($a^-a^-c^0$)	$a \approx \sqrt{2}a_p$ $b \approx \sqrt{2}a_p$ $c \approx 2a_p$	4*e* (x,0,¼) x ≈ ½	4*a* (0,0,0)	4*e* (x,0,¼) x ≈ 0 8*g* (¼,¼,z) z ≈ 0
$R\bar{3}c$ ($a^-a^-a^-$)	$a = b = c \approx \sqrt{2}a_p$ $\alpha = \beta = \gamma \approx 60°$	2*a* (¼,¼,¼)	2*b* (0,0,0)	6*e* (x,½-x,¼) x ≈ ¾

Space Group (Tilt System)	Unit-cell Size	Atomic Positions (Wyckoff Symbol, Co-ordinates)		
		A	B	O
*C*2/*m* ($a^-b^-c^0$)	$a \approx 2a_p$ $b \approx 2a_p$ $c \approx \sqrt{2}a_p$ $\beta \neq 90°$	4*i* (x,0,z) x ≈ ¼, z ≈ ½	4*e* (¼,¼,0)	4*h* (0,y,½) y ≈ ¼ 4*g* (0,y,0) y ≈ ¾ 4*i* (x,0,z) x ≈ ¼, z ≈ 0
*I*2/*a* ($a^-b^-b^-$)	$a \approx 2a_p$ $b \approx \sqrt{2}a_p$ $c \approx \sqrt{2}a_p$ $\beta \neq 90°$	4*e* (¼,y,0) y ≈ 0	4*b* (0,½,0)	4*e* (¼,y,0) y ≈ ½ 8*f* (x,y,z) x ≈ 0, y ≈ ¼, z ≈ ¼
$I\bar{1}$ ($a^-b^-c^-$)	$a \approx \sqrt{2}a_p$ $b \approx \sqrt{2}a_p$ $c \approx 2a_p$ $\alpha \neq \beta \neq \gamma \neq 90°$	4*i* (x,y,z) x ≈ 0, y ≈ ½, z ≈ ¼	2*a* (0,0,0) 2*e* (0,0,½)	4*i* (x,y,z) x ≈ 0, y ≈ 0, z ≈ ¼ 4*i* (x,y,z) x ≈ ¼, y ≈ ¾, z ≈ 0 4*i* (x,y,z) x ≈ ¾, y ≈ ¾, z ≈ ½
Cmcm ($a^0b^-c^+$)	$a \approx 2a_p$ $b \approx 2a_p$ $c \approx 2a_p$	4*c* (0,y,¼) y ≈ 0 4*c* (0,y,¼) y ≈ ½	8*d* (¼,¼,0)	8*e* (x,0,0) x ≈ ¼ 8*f* (0,y,z) y ≈ ¼, z ≈ 0 8*g* (x,y,¼) x ≈ ¼, y ≈ ¼
Pnma ($a^-b^+a^-$)	$a \approx \sqrt{2}a_p$ $b \approx 2a_p$ $c \approx \sqrt{2}a_p$	4*c* (x,¼,z) x ≈ ½, z ≈ 0	4*a* (0,0,0)	4*c* (x,¼,z) x ≈ 0, z ≈ 0 8*d* (x,y,z) x ≈ ¼, y ≈ 0, z ≈ ¼
Pbnm ($a^-a^-c^+$)	$a \approx \sqrt{2}a_p$ $b \approx \sqrt{2}a_p$ $c \approx 2a_p$	4*c* (x,y,¼) x ≈ 0, y ≈ ½	4*a* (0,0,0)	4*c* (x,y,¼) x ≈ 0, y ≈ 0 8*d* (x,y,z) x ≈ ¼, y ≈ ¼, z ≈ 0
$P2_1/m$ ($a^-b^+c^-$)	$a \approx \sqrt{2}a_p$ $b \approx 2a_p$ $c \approx \sqrt{2}a_p$ $\beta \neq 90°$	2*e* (x,¼,z) x ≈ 0, z ≈ 0 2*e* (x,¼,z) x ≈ ½, z ≈ ½	2*b* (½,0,0) 2*c* (0,0,½)	2*e* (x,¼,z) x ≈ 0, z ≈ ½ 2*e* (x,¼,z) x ≈ ½, z ≈ 0 4*f* (x,y,z) x ≈ ¼, y ≈ 0, z ≈ ¼ 4*f* (x,y,z) x ≈ ¼, y ≈ 0, z ≈ ¾
$P4_2/nmc$ ($a^+a^+c^-$)	$a \approx 2a_p$ $b \approx 2a_p$ $c \approx 2a_p$	2*a* (¾,¼,¾) 2*b* (¼,¼,¼) 4*d* (¼,¼,z) z ≈ ¼	8*e* (0,0,0)	8*g* (¼,y,z) y ≈ 0, z ≈ 0 8*g* (¼,y,z) y ≈ ½, z ≈ ½ 8*f* (x,-x,¼) x ≈ ½

Recently Howard and Stokes[9] used group theoretical analysis to obtain 15 possible tilt systems for ternary perovskites (see Table 1.1 for Wyckoff crystallographic positions). The difference in the number of tilt systems between this work and that proposed by Glazer is caused by some of Glazer's arrangements requiring higher symmetry than those imposed by the space group[9]. Howard and Stokes argued such tilt systems would not occur in a real crystal. Howard and Stokes[9] also used the Lifshitz criterion and Landau theory to establish which transitions between space groups with a group-subgroup relationship are required to be first order (discontinuous) and which are allowed to be continuous (see Figure 1.4). Perovskites of lower symmetry can usually be made to undergo a series of phase transitions to a

higher symmetry by either increasing the size of the A-site cation compared to the B-site cation or by increasing the temperature. These actions both reduce the need for octahedral tilting and ultimately lead to the primitive cubic structure. There are, however, usually several alternate routes that can be taken to reach $Pm\bar{3}m$ symmetry and the forces that drive perovskites to adopt one sequence of phase transitions compared to another are not well understood. The nature of phase transitions in perovskites is important as first order transformations can lead to the delamination and deterioration of devices frequently heated or cooled through the transition. Understanding the nature of any transitions is crucial to the optimisation of perovskites in applied devices.

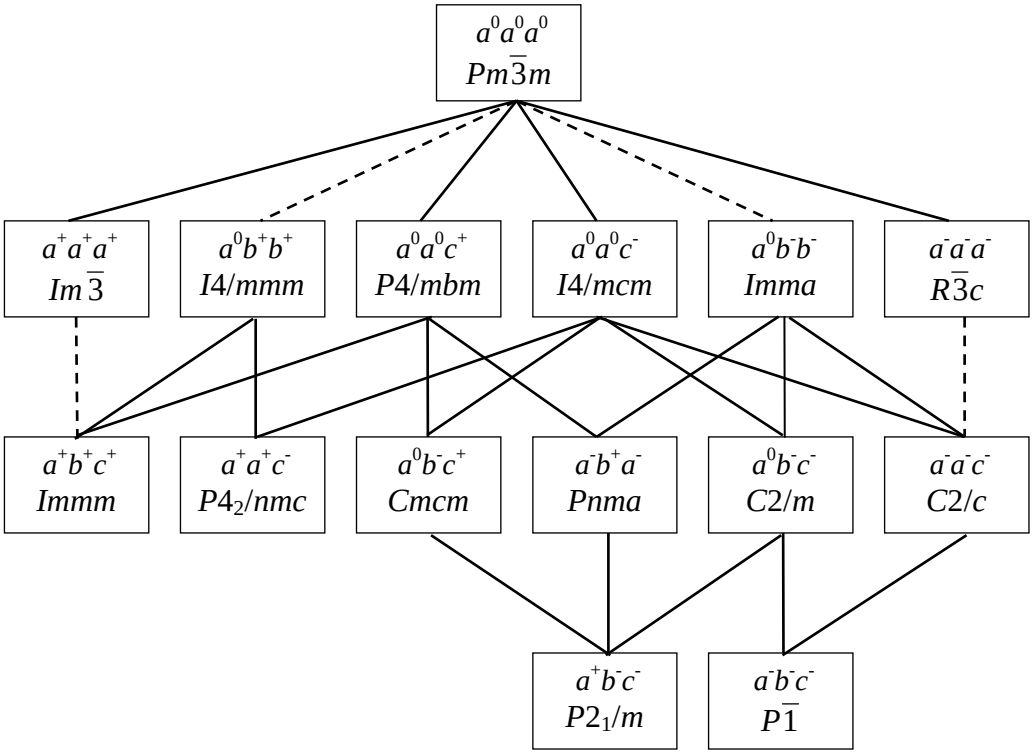

Figure 1.4: Diagram indicating the 15 space groups that encompass the possible symmetries caused by octahedral tilting in perovskites. The presence of a line between space groups indicate where a group-subgroup relationship exists. A solid line signifies a transition that is allowed to be continuous and a dashed line or no line between space groups indicates a transition that is required to be first order. This diagram is modified from Howard and Stokes[9].

Further complicating the possible structures of perovskites is the observation that two or more cations may share the A- or B-sites[2]. This can be in either a disordered or ordered manner. Double perovskites are an example of such an ordered arrangement where the B-sites are occupied by two different cations. Two possible motifs of 1:1 B-site ordering are possible, in either a rock salt or a layered fashion (see Figure 1.5)[2]. Layered ordering is extremely rare while rock salt ordering is very common, so the term double perovskite will be used here onwards to only refer to rock salt ordered compounds. This ordering can be complete or partial depending on the charge and ionic radii difference of the two cations. The degree of ordering tends to increase with increasing size and charge difference. Any ordering leads to a change in the symmetry so that there are two distinct B-cation sites. The undistorted cubic structure in this case is $Fm\bar{3}m$ and distortions to the double perovskite structure occur in the same three ways as for the primitive cubic perovskite structure.

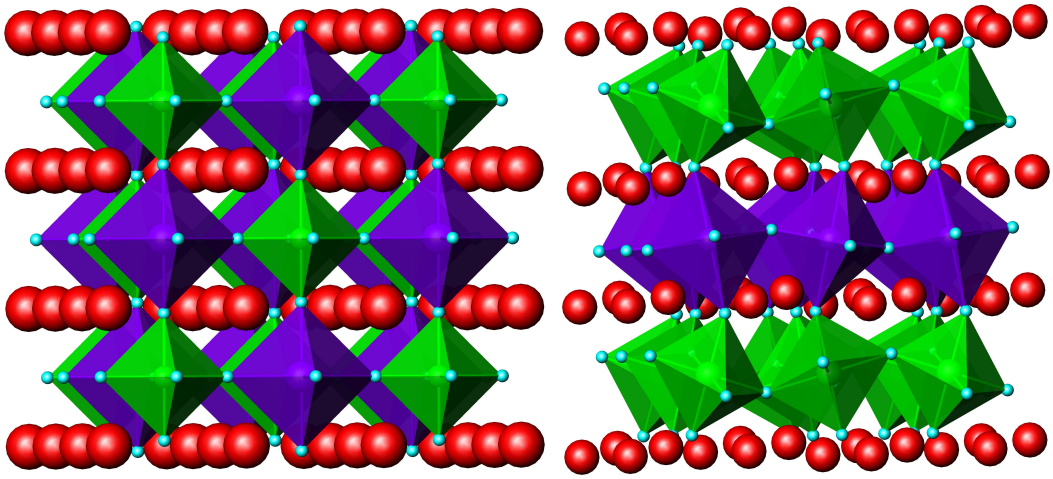

Figure 1.5: The two alternate types of ordering known to occur in $A_2BB'O_6$ perovskites; the untilted variant of the rock salt ordered structure (left) and the layered ordering first found to be adopted by La_2CuSnO_6 (right)[10].

Octahedral tilting is also the most common distortion from the undistorted double perovskite structure. A recent group-theoretical analysis by Howard *et al.*[11] has indicated there are 12 possible space groups for double perovskites featuring only distortions from the cubic structure by octahedral tilting (see Figure 1.6 for group-subgroup relationships and Table 1.2 for crystallographic details). These were ordered by group-subgroup relationships and Landau theory was used to determine if the

phase transitions between these space groups are required to be first order or if they are allowed to be second order in nature.

Table 1.2: Unit cell descriptions and atomic positions for all the space groups generated by tilting of the BO_6 octahedra of the ideal cubic double perovskite. The majority of structures described use the settings of the space groups employed by Howard *et al.*[11]. For tilt systems $a^-a^-c^0$, $a^-b^-c^-$ and $a^-a^-c^+$, however, the more commonly used $I2/m$, $I\bar{1}$ and $P2_1/n$ settings are detailed. a_p is the unit cell length of the primitive cubic structure and the tilt system given is specific to the crystallographic setting of the space group described.

Space Group (Tilt System)	Unit-cell Size	Atomic Positions (Wyckoff Symbol, Co-ordinates)		
		A	B	O
$Fm\bar{3}m$ ($a^0a^0a^0$)	$a = b = c \approx 2a_p$	8*c* (¼,¼,¼)	4*a* (0,0,0) 4*b* (½,½,½)	24*e* (x,¼,¼) x ≈ ¼
$P4/nmc$ ($a^0a^0c^+$)	$a = b \approx \sqrt{2}a_p$ $c \approx 2a_p$	4*d* (0,½,¼)	2*a* (0,0,0) 2*b* (0,0,½)	4*e* (0,0,z) z ≈ ¼ 8*h* (x,y,0) x ≈ ¼, y ≈ ¾
$P4_2/nnm$ ($a^0b^+b^+$)	$a \approx 2a_p$ $b = c \approx 2a_p$	2*a* (¼,¾,¼) 2*b* (¾,¼,¼) 2*c* (¼,¼,¼)	4*f* (0,0,0) 4*e* (0,0,½)	8*m* (x,$\bar{x}$,z) x ≈ 0, z ≈ ¼ 16*n* (x,y,z) x ≈ 0, y ≈ ¼, z ≈ 0
$Pn\bar{3}$ ($a^+a^+a^+$)	$a = b = c \approx 2a_p$	2*a* (¼,¼,¼) 6*d* (¼,¾,¾)	4*b* (0,0,0) 4*c* (½,½,½)	24*h* (x,y,z) x ≈ ¼, y ≈ 0, z ≈ 0
$Pnnn$ ($a^+b^+c^+$)	$a \approx 2a_p$ $b \approx 2a_p$ $c \approx 2a_p$	2*a* (¼,¼,¼) 2*b* (¾,¼,¼) 2*c* (¼,¼,¾) 2*d* (¼,¾,¼)	4*f* (0,0,0) 4*e* (½,½,½)	8*m* (x,y,z) x ≈ ¾, y ≈ 0, z ≈ 0 8*m* (x,y,z) x ≈ 0, y ≈ ¼, z ≈ 0 8*m* (x,y,z) x ≈ 0, y ≈ 0, z ≈ ¼
$I4/m$ ($a^0a^0c^-$)	$a = b \approx \sqrt{2}a_p$ $c \approx 2a_p$	4*d* (0,½,¼)	2*a* (0,0,0) 2*b* (0,0,½)	4*e* (0,0,z) z ≈ ¼ 8*h* (x,y,0) x ≈ ¼, y ≈ ¼
$I2/m$ ($a^-a^-c^0$)	$a \approx \sqrt{2}a_p$ $b \approx \sqrt{2}a_p$ $c \approx 2a_p$ $\beta \neq 90°$	4*i* (x,0,z) x ≈ ½, z ≈ ¼	2*a* (0,0,0) 2*d* (0,0,½)	4*i* (x,0,z) x ≈ 0, z ≈ ¼ 8*j* (x,y,z) x ≈ ¼, y ≈ ¼, z ≈ 0
$R\bar{3}$ ($a^-a^-a^-$)	$a = b = c \approx \sqrt{2}a_p$ $\alpha = \beta = \gamma \approx 60°$	2*c* (x,x,x) x ≈ ¼	1*a* (0,0,0) 1*b* (½,½,½)	6*f* (x,y,z) x ≈ ¾, y ≈ ¼, z ≈ ¼
$I\bar{1}$ ($a^-b^-c^-$)	$a \approx \sqrt{2}a_p$ $b \approx \sqrt{2}a_p$ $c \approx 2a_p$ $\alpha \neq \beta \neq \gamma \neq 90°$	4*i* (x,y,z) x ≈ 0, y ≈ ½, z ≈ ¼	2*a* (0,0,0) 2*g* (0,0,½)	4*i* (x,y,z) x ≈ 0, y ≈ 0, z ≈ ¼ 4*i* (x,y,z) x ≈ ¼, y ≈ ¼, z ≈ 0 4*i* (x,y,z) x ≈ ¼, y ≈ ¾, z ≈ 0
$C2/c$ ($a^0b^+c^-$)	$a \approx 2a_p$ $b \approx 2a_p$ $c \approx 2a_p$ $\beta \neq 90°$	4*e* (0,y,¼) y ≈ 0 4*e* (0,y,¼) y ≈ ½	4*c* (¼,¼,0) 4*d* (¼,¼,½)	8*f* (x,y,z) x ≈ ¼, y ≈ 0, z ≈ 0 8*f* (x,y,z) x ≈ 0, y ≈ ¼, z ≈ 0

Space Group (Tilt System)	Unit-cell Size	Atomic Positions (Wyckoff Symbol, Co-ordinates)		
		A	B	O
				8*f* (x,y,z) x ≈ ¼, y ≈ ¼, z ≈ ¼
$P2_1/n$ ($a^-a^-c^+$)	$a \approx \sqrt{2}a_p$ $b \approx \sqrt{2}a_p$ $c \approx 2a_p$ $\beta \neq 90°$	4*e* (x,y,z) x ≈ 0, y ≈ ½, z ≈ ¼	2*a* (0,0,0) 2*b* (0,0,½)	4*e* (x,y,z) x ≈ 0, y ≈ 0, z ≈ ¼ 4*e* (x,y,z) x ≈ ¼, y ≈ ¼, z ≈ 0 4*e* (x,y,z) x ≈ ¼, y ≈ ¾, z ≈ 0
$P4_2/n$ ($a^+a^+c^-$)	$a = b \approx 2a_p$ $c \approx 2a_p$	2*a* (¼,¼,¼) 2*b* (¼,¼,¾) 4*e* (¾,¼,z) z ≈ ¼	4*c* (0,0,0) 4*d* (0,0,½)	8*g* (x,y,z) x ≈ ¼, y ≈ 0, z ≈ 0 8*g* (x,y,z) x ≈ 0, y ≈ ¼, z ≈ 0 8*g* (x,y,z) x ≈ 0, y ≈ 0, z ≈ ¼

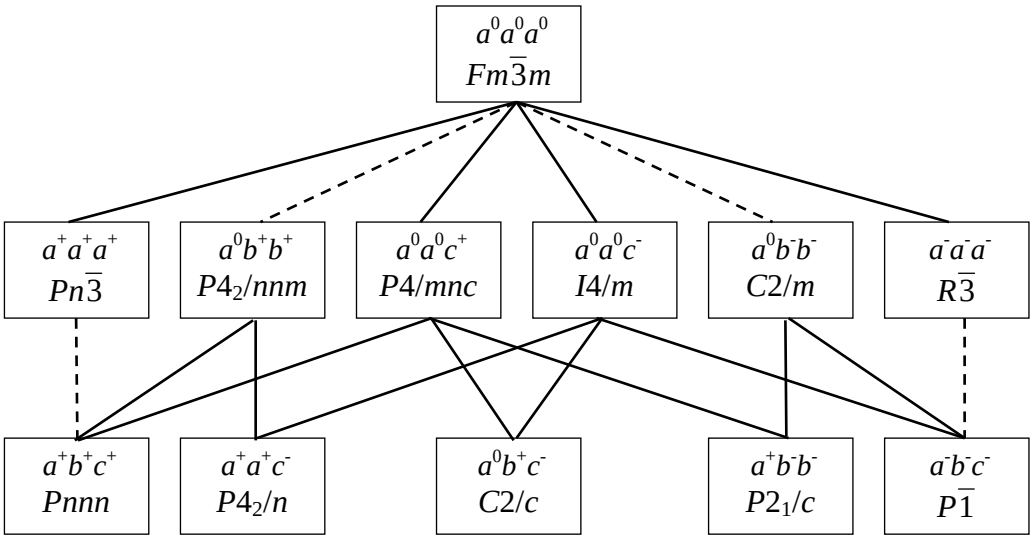

Figure 1.6: Diagram indicating the 12 space groups that encompass the possible symmetries caused by octahedral tilting in double perovskites. The format is the same as Figure 1.4. The diagram is reproduced from Howard *et al.*[11].

1.3 Physical and Chemical Influences on the Perovskite Structure

In the previous section the ideal cubic perovskite structure was discussed and the ways that perovskites can vary from this ideal were reviewed with a particular focus on the most common form of distortion; octahedral tilting. Following on from this the chemical reasons behind such distortions will now be described, starting from the

ternary ABO_3 perovskites that have been more thoroughly studied and then, in the following section, the differences in the tilted structures adopted by ternary and double perovskites will be examined. As mentioned above, the tolerance factor, *t*, provides an indication of how suitable a perovskite structure will be for a certain combination of A- and B-site cations and provides an, albeit limited, insight into how large a distortion from the ideal perovskite structure is likely to be required to accommodate a particular combination of cations. It does not, however, provide any information about the precise nature of the distortion. Randall *et al.*[12] indicated that ternary perovskites exist over the range $1.05 > t > 0.78$. ABO_3 compounds with *t* values outside this range form other structures such as the ilmenite structure for low values of *t* and hexagonal closed-packed perovskites for higher values of *t* (see Figure 1.7)[1, 13, 14]. Where the perovskite structure is observed compounds with a low value of *t* will generally be distorted from the cubic structure by octahedral tilting, while those with too high a value of *t* will often have their B-site cation displaced from the centre of the octahedra, as is the case for the widely used ferroelectric $BaTiO_3$[14].

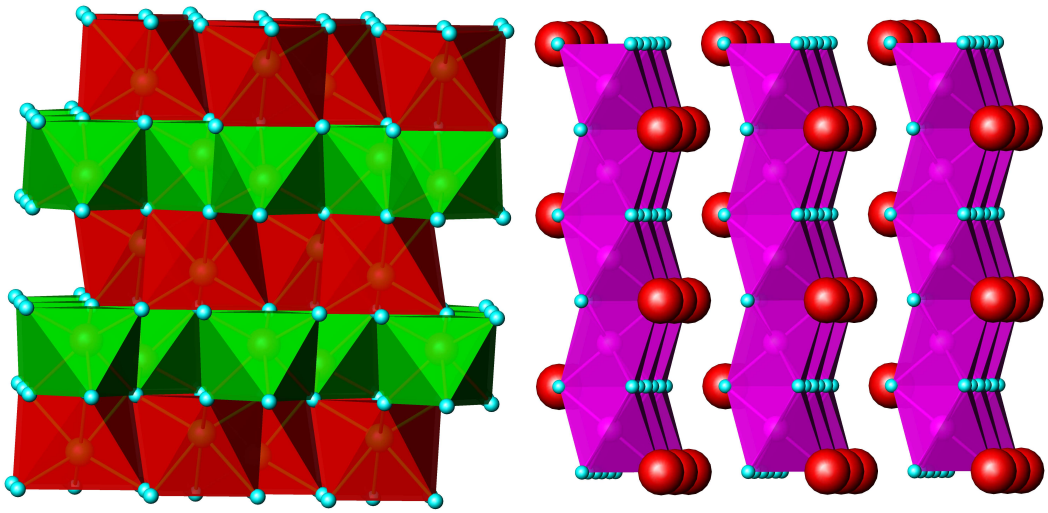

Figure 1.7: Images of the octahedral face sharing structures of ilmenite (left) and 2H hexagonal perovskite (right) structures.

B-site cation displacement commonly occurs in perovskites that have tolerance factors that are too large and where the B-site cation is a transition metal with a d^0 electronic configuration such as $BaTiO_3$ and $NaNbO_3$[1, 6, 14]. This distortion leads to one or more B-O bonds becoming shorter while the other B-O bond lengths become longer. These shortened bond lengths better satisfy the bonding requirements of the

B-site cation since the strength of a bond is exponentially related to the distance between the cation and the anion[15]. Since the increase in the strength of the shortened B-O bonds is greater than the decrease in the strength of the lengthened B-O bonds this distortion leads to an increase in the overall bonding strength of the B-site cation. This effect is best quantified by the bond valence concept developed by Brown and Altermatt[15] that calculates the strengths of individual cation-anion bonds using Equation 1.2 where v_{ij} is the bond valence, d_{ij} is the bond distance, R_{ij} is the bond valence parameter for a particular cation and anion combination and b is a "universal constant" (equal to 0.37 Å). Bond valence sums represent a more accurate measure of a cations (or anions) total bonding strength than is the case for ionic radius particularly for a cation in an asymmetric bonding environment.

$$v_{ij} = exp\frac{R_{ij} - d_{ij}}{b} \qquad \textbf{1.2}$$

Displacement of the B-site cation is not, however, favoured for perovskites where the B-site cation is either a main group metal or a transition metal with occupied *d*-orbitals. This is because the displacement of the B-site cation leads to lowering of the energy of the valence band that acts to stabilise the structure in the d^0 case, but also increases the energy level of the π* orbitals[16]. Since the π* orbitals are, at least partially, occupied for d^n transition metals with $n \geq 1$ and for the main group metals, the increased energy of the π*-band makes the B-site cation displacement unfavourable in such compounds. It should also be mentioned that having an A-site cation with a lone pair of *s*-electrons e.g. Pb^{2+} or Bi^{3+} tends to lead to a larger B-site cation displacement as a result of the attraction between the lone pair and the B-site cation[1]. These observations highlight the limitations of using a simple, purely ionic, model to examine bonding in perovskites, and illustrates the importance of both covalent bonding and the electronic configuration of the cations. Similarly the most common case where the BO_6 bond lengths are distorted from a regular octahedra without B-site cation displacement is the Jahn-Teller distortion. This is associated with cations such as Mn^{3+} and Cu^{2+}, which have unequally filled e_g-orbitals and is, therefore, an electronic effect[1].

Table 1.3: List of the ternary perovskite tilt systems divided into those containing one, and those containing more than one, crystallographic A-site. The number in square brackets in the right-hand column is the number of crystallographic A-sites in each space group.

Tilt Systems with 1 Crystallographic A-site	Tilt Systems with more than 1 Crystallographic A-site
$Pm\bar{3}m$ ($a^0a^0a^0$)	$I4/mmm$ ($a^0b^+b^+$) [3]
$I4/mcm$ ($a^0a^0c^-$)	$Cmcm$ ($a^0b^-c^+$) [2]
$P4/mbm$ ($a^0a^0c^+$)	$Im\bar{3}$ ($a^+a^+a^+$) [2]
$Imma$ ($a^0b^-b^-$)	$P2_1/m$ ($a^+b^-c^-$) [2]
$C2/m$ ($a^0b^-c^-$)	$P4_2/nmc$ ($a^+a^+c^-$) [3]
$R\bar{3}c$ ($a^-a^-a^-$)	$Immm$ ($a^+b^+c^+$) [4]
$C2/c$ ($a^-a^-c^-$)	
$Pnma$ ($a^-b^+a^-$)	
$P\bar{1}$ ($a^-b^-c^-$)	

Octahedral tilting, the third type of distortion of the perovskite structure, usually occurs when the A-site cation is too small compared to the B-site cation. The type of rotation adopted is mainly driven by the optimisation of the bonding environments of the A-site cation. In this context the fifteen possible tilt systems adopted by ternary perovskites can be broken up into two groups. There are structures where all the A-sites are crystallographically identical and those where there are two or more crystallographically different A-sites[9, 17]. Despite accounting for 40 % of the possible tilt systems (see Table 1.3) only 7 % of known ternary perovskites adopt tilt systems with more than one crystallographically different A-site cation (see Table 1.4). Perovskites adopting one of these structures either do so over a narrow temperature range, as is the case for *Cmcm* (tilt system $a^0b^-c^+$), or are stabilised by having two very different A-site cations, as is the case for $P4_2/nmc$ ($a^+a^+c^-$) e.g. $CaFeTi_2O_6$ and $Im\bar{3}$ ($a^+a^+a^+$) e.g. $CaCu_3M_4O_{12}$ (where M = Ge^{4+}, Mn^{4+}, Ti^{4+} or Ru^{4+})[13, 18]. The later category of compounds generally requires synthesis at high pressures in order to fit the small A-site cation e.g. Fe^{2+} or Cu^{2+} into the structure. That tilt systems with more than one crystallographic A-site are relatively rare is not surprising as it fits well with the physiochemical concept stated by Pauling's rule of parsimony[19]. This concludes

that the number of chemically different environments in a crystal tends to be small. This occurs because the structure will distort in the same way throughout to achieve the same optimal co-ordination for each type of A-site cation. It is only when A-site cations are significantly different that a structure with more than one A-cation site becomes stable over a wide temperature range.

Understanding the reasons for the different stability of the other eight tilt systems requires a careful consideration of bonding in the perovskite structure, particularly in regards to the A-site cation. The bonding of the A-site cation can be considered using either an ionic or covalent model. Woodward[13] examined both these approaches using lattice energy and extended Hückel calculations to model ionic and covalent bonding in $YAlO_3$. The ionic model suggested that, as is in fact experimentally observed, *Pnma* ($a^-b^+a^-$) symmetry was the most stable followed closely by $R\bar{3}c$ ($a^-a^-a^-$) and then *Imma* ($a^0b^-b^-$)[13, 20]. These calculations revealed that $R\bar{3}c$ had both the strongest attractive and repulsive forces while the undistorted cubic structure minimises the repulsive term. In this case *Pnma* symmetry was found to be the most stable since it achieved the best balance between attractive and repulsive forces. Woodward interpreted these results to indicate that bonding in the ionic model favours rhombohedral symmetry where the repulsive term is small i.e. the A-site cation has a high charge and the compound has a tolerance factor in the range 0.975-1.00. For larger *t*, cubic symmetry is favoured since the A-cation is too large leading to increased repulsive forces that the cubic structure reduces. On the other hand when *t* is smaller repulsion also becomes important since the larger degree of octahedral tilting leads to very short A-O bond lengths. This favours *Pnma* symmetry since it has similar coulomb attractive forces to rhombohedral symmetry but less ion-ion repulsion. Woodward also noted that the energy stabilisation from the coulomb attraction in the rhombohedral structure decreases as the A-site cation charge decreases. This is consistent with the $A^{3+}M^{3+}O_3$ perovskites adopting rhombohedral symmetry either at room temperature or as an intermediate between orthorhombic and cubic symmetry with increasing temperature while the $A^{2+}M^{4+}O_3$ compounds commonly adopt *I*4/*mcm* symmetry[1, 13].

Table 1.4: Space groups and relative abundance of each of the Glazer tilt systems adopted by compounds with the ternary and double perovskite structures. Relative abundances were determined by a thorough search of the ICSD[21]. All settings of each tilt system were included in this analysis. The number in square brackets next to the space group is the number of crystallographic A-sites in each structure.

Tilt System	Space Group for Ternary Perovskite	Percentage of Total Ternary Perovskites (%)	Space Group for Double Perovskite	Percentage of Total Double Perovskites (%)
$a^0a^0a^0$	$Pm\bar{3}m$ [1]	29.0	$Fm\bar{3}m$ [1]	51.7
$a^0a^0c^-$	$I4/mcm$ [1]	4.3	$I4/m$ [1]	7.9
$a^0a^0c^+$	$P4/mbm$ [1]	1.1	$P4/mnc$ [1]	0.2
$a^-a^-c^0$	$Ibmm$ [1]	3.1	$I2/m$ [1]	4.0
$a^0b^-c^+$	$Cmcm$ [2]	0.6	$C2/c$ [2]	0.2
$a^0b^+b^+$	$I4/mmm$ [3]	0.2	$P4_2/nnm$ [3]	0
$a^-a^-a^-$	$R\bar{3}c$ [1]	9.4	$R\bar{3}$ [1]	3.2
$a^-b^-c^-$	$P\bar{1}$ [1]	0.1	$P\bar{1}$ [1]	0.8
$a^-a^-c^+$	$Pbnm$ [1]	45.9	$P2_1/n$ [1]	31.5
$a^+a^+c^-$	$P4_2/nmc$ [3]	0.1	$P4_2/n$ [3]	0
$a^+b^+c^+$	$Immm$ [4]	0	$Pnnn$ [4]	0
$a^+a^+a^+$	$Im\bar{3}$ [2]	4.8	$Pn\bar{3}$ [2]	0.6
$a^0b^-c^-$	$C2/m$ [1]	0.1	N/A	
$a^-a^-c^-$	$C2/c$ [1]	0.7	N/A	
$a^+b^-c^-$	$P2_1/m$ [2]	0.6	N/A	

Examination using a covalent model of the A-O bonding also indicated that *Pnma* symmetry was the most stable followed by *Imma* and $R\bar{3}c$ [13]. Covalent bonding favours *Pnma* symmetry because it maximises the number of oxygen atoms that the A-site cation can co-ordinate since the first co-ordination sphere of oxygen atoms is non-planar in this structure. *Imma* symmetry was found to be favoured over rhombohedral symmetry for the same reason. It should be noted that these calculations do not allow a comparison between the relative importance of ionic or covalent bonding for the A-site cation. They do, however, show that A-site bonding favours *Pnma* (alternatively set as *Pbnm*), $R\bar{3}c$ and *Imma* (alternatively set as *Ibmm*)

symmetries, which are three of the four most commonly observed tilted perovskite structures featuring only one crystallographic A-site[18].

While A-site bonding is generally regarded as the driving force for octahedral tilting in perovskites, because the energy difference between the various tilt systems is small the bonding of the B-site cation must also play a role in determining the tilt system adopted[1, 16]. Woodward[13] examined B-O bonding in the ternary perovskite structure using extended Hückel calculations. These calculations showed that the σ- and π-bonding strength of the B-O bonds decrease at approximately the same rate as the B-O-B bond angle decreases. This indicates that, from a B-O bonding viewpoint, structures with the straightest bonding angles will be favoured, e.g. the untilted cubic structure, due to better orbital overlap of the B-site cation and oxygen anion bonding orbitals. Despite this, the vast majority of perovskites where the B-site cation is a *p*-block metal adopt tilted structures even when $t \approx 1$[13]. Apparently, in the absence of π-bonding the σ-bonding of the B-site cation is unable to offset the energy gain derived from the A-site bonding in the tilted structure[13].

Conversely Woodward found that where the tolerance factor is high, t > 0.98, and π-bonding is present the stability of the cubic structure is considerably enhanced, compared to tilted structures, where the B-O-B bond angle is not 180°[13]. The stabilisation of the cubic structure by π-bonding was largest for transition metals with only a small number of *d*-electrons i.e. d^1 to d^3 and decreases after this[13]. This occurs because the straighter B-O-B linkages lead to a better overlap of the B-cation *d*- and oxygen *p*-orbitals leading to a wider π*-band for the cubic structure. Assuming that the centre of the π*-band is at the same energy, the wider band of the cubic structure leads to the bottom of the π*-band being lower in energy than is the case for the narrower band (see Figure 1.8). Therefore, while the bottom half of this band is being filled the structure with straighter B-O-B angles is stabilised relative to the structure where the bond angle is not 180°. If the two bands are centred at the same energy the maximum stabilisation of the cubic structure will occur for d^3 with any further filling of the π*-band leading to a relative destabilisation of the cubic structure[13]. It should be noted, however, that the narrow band is usually slightly lower in energy than the wide band because of the poorer B-O orbital overlap in the structure with bent B-O-B

bonds. This leads to the maximum stabilisation of the cubic structure being shifted to a lower number of *d*-electrons.

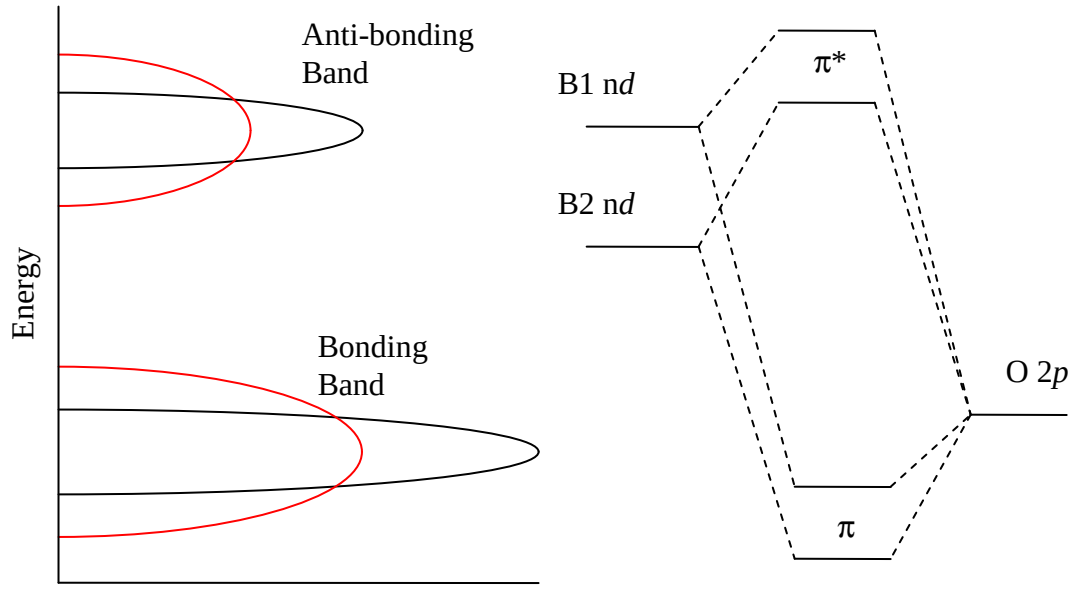

Figure 1.8: Illustration of the effect of decreased B-O-B bond angle on the bonding and anti-bonding orbital bandwidths (left) and the effect of increasing electronegativity of the B-cation from B1 to B2 on the energy of the π and π*-orbitals (right). In the band diagram the red bands are wider than the black bands because of the straighter B-O-B bond angle in this case.

Increasing the electronegativity of the B-site cation results in stronger B-O interactions leading to an increase in the energy level of the π*-band relative to non-bonding bands (see Figure 1.8). This favours the structure with the most bent B-O-B bond angles, since the bending of the B-O-B bond angle leads to a smaller amount of orbital overlap consequently reducing the anti-bonding character of the π*-band[13]. While Woodward framed his argument in the context of stabilising the untilted cubic structure compared to the *Pnma* structure, it is reasonable to conclude that where the B-site cation is a transition metal with a small number of *d*-electrons tilted structures that have B-O-B bond angles close to 180° will be favoured by B-site cation π-bonding, compared to those structures where the B-O-B bond angle is less straight. This may be why *I*4*/mcm* symmetry is found as an intermediate structure rather than $R\bar{3}c$ between orthorhombic and cubic symmetry where the B-site cation is

a transition metal with a small number of *d*-electrons e.g. $SrTiO_3$, $SrZrO_3$ and $La_{0.5}Sr_{0.5}MnO_3$[1].

1.4 Comparison between Tilted Structures in Ternary and Double Perovskites

Just as there are many similarities between the tilted structures adopted by ternary and double perovskites there are also significant differences between the relative abundance of the tilt systems adopted by these compounds. To date, there has been little work reported into understanding the differences in the stabilising forces between ternary and double perovskites. While such a comparison is out of the scope of the current thesis, a comparison between the relative abundance of the various space groups in ternary and double perovskites may, at least, provide a useful basis for explaining the stability of different ternary and double perovskites. The relative abundance of the various tilt systems of both ternary and double perovskites in the Inorganic Crystal Structure Database[21] is given in Table 1.4. This table includes all perovskite-type structures that belong to each of the space groups adopted by the ternary and double perovskites including structures with cation and anion vacancies, where these do not change the symmetry of the structure, and solid solutions. In the case of solid solutions multiple entries of the same space group were treated as a single entry as long as the same combination of elements was present. Similarly multiple reports of a particular composition at different temperatures adopting the same space group were treated as a single entry.

The most obvious difference between the tilt systems adopted by ternary and double perovskites is that, according to the group theoretical analysis of Howard *et al.*[9, 11], there are three tilt systems adopted by ternary perovskites that are not adopted by their double perovskite analogues; namely $a^-a^-c^-$, $a^0b^-c^-$ and $a^+b^-c^-$. Double perovskites do not adopt these tilt systems as they are incompatible with rock-salt ordering. These three tilt systems, however, account for less than 2 % of all reported ternary tilted perovskites so their absence in the double perovskites does not significantly affect the abundance of the other 12 structures.

The most striking difference between the relative abundance of the double perovskite structures and that of their ternary counterparts is the fraction of compounds found to adopt the untilted structure. In the ternary perovskites the untilted $Pm\bar{3}m$ structure accounts for about 29 % of known tilted perovskites, while for the double perovskites the corresponding $Fm\bar{3}m$ structure accounts for over half the double perovskites. In particular nearly all halides with the double perovskite structure are reported to adopt $Fm\bar{3}m$ symmetry whereas about half of the ternary halide perovskites adopt the primitive cubic structure. This difference is also matched by an increased tolerance factor range in the double perovskites over which the untilted structure exists compared to the ternary cubic structure. The increased number of perovskites with a tolerance factor over one has been explained, by Lufaso *et al.*[22], as being a consequence of the existence of very few double perovskite structures that have B-site cation displacements, which typically occur for ternary perovskites with similar tolerance factors. They suggest this occurs because in a double perovskite typically only one of the B-site cations present has the d^0 electronic configuration required to stabilise such a distortion. Furthermore the oxygen anion now has some, albeit limited, flexibility to move.

Some of the difference in the relative abundance of the untilted ternary and double perovskite structures may also be caused by compounds that have been assigned an incorrect structure. This is particularly likely since many perovskites have only been prepared in a polycrystalline form with the structure of many of these compounds being determined by conventional (laboratory) X-ray diffraction. The high degree of pseudo-symmetry of perovskites means that it is likely that some of these compounds will have been incorrectly assigned as having a higher symmetry than they actually possess. While this may effect the abundance of all the different perovskite variants the most likely incorrect assignments would be to the highest symmetry cubic structure. This would increase the number of reported undistorted cubic ternary and double perovskite structures. Clearly it is important to grow single crystals of these materials and determine their structure using single crystal diffraction or, as is more practical in many cases, use a combination of high resolution neutron and synchrotron X-ray powder diffraction. Either of these alternatives allows the structure of a perovskite to be accurately and precisely determined.

The relative abundance of ternary and double perovskites with more than one crystallographic A-site is also significantly different. While ternary perovskites with these structures are relatively uncommon there are even fewer reports of these structures for double perovskites. This difference may point to another limitation in using these statistics to compare the two types of compounds since all the known double perovskites with more than one A-site have been discovered relatively recently[23, 24]. This suggests that their relative rarity may be a results of insufficient research in this area particularly since almost all ternary and double perovskites with these sorts of structures either require high pressure synthesis or exist over a very narrow temperature range[18, 23, 24].

Finally, it is interesting to note that in both the ternary and double perovskites the five most common tilt systems with only one A-cation site are $a^0a^0a^0$, $a^-a^-b^+$, $a^0a^0c^-$, $a^-a^-a^-$ and $a^-a^-c^0$. The relative abundance of the $a^-a^-a^-$ and $a^0a^0c^-$ tilt systems changes significantly between ternary and double perovskites. In the ternary perovskites the $a^-a^-a^-$ system is far more common than it is in the double perovskites while in the double perovskites $a^0a^0c^-$ is more common. This may be related to the $a^-a^-a^-$ tilt system being associated most commonly with A^{3+} containing perovskites with intermediate tolerance factor values (t > 0.96), which are rarer in the double perovskite family than for the ternary perovskite compounds[1, 17]. The A^{2+} perovskites are more common in the double perovskites than in the ternary perovskites and tend to adopt the $a^0a^0c^-$ tilt system. Most of the known double perovskites with the $a^-a^-a^-$ tilt system contain A^{2+} cations so clearly the forces that determine which symmetry is adopted are more complicated than simple electrostatic arrangement[1, 22]. It has been noted that the A^{2+} double perovskites with the $a^-a^-a^-$ tilt system ($R\bar{3}$ symmetry) usually contain a main group metalloid such as Sb^{5+} or Bi^{5+} as one of the B-site cations[1, 22]. On the other hand, the majority of those double perovskites adopting $a^0a^0c^-$ tilting ($I4/m$ symmetry) containing transition metals commonly have at least one cation with a small number of *d*-electrons e.g. W^{6+}, Mo^{6+}, $Nb^{5+}$and Ta^{5+}. It is expected that structural studies of compounds with similar electrostatic arrangements and ionic radii, but different preferences for these two tilt systems will shed further light on why rhombohedral symmetry is preferred compared to tetragonal symmetry

in some cases but not others. One such series is $Ba_2LnB'O_6$ (B' = Nb^{5+}, Ta^{5+}, Mo^{5+}, Ru^{5+}, Ir^{5+}, Bi^{5+} or Sb^{5+}) in which some of the compounds adopt a rhombohedral structure and others adopt tetragonal symmetry as an intermediate phase between monoclinic and cubic symmetries depending on the choice of B' cation[25-30]. This series has been selected for study in this project in order to better understand the relative stability of the rhombohedral and tetragonal structures in double perovskites and the results from this structural study will be presented in Chapters 3 and 4.

1.5 Oxygen Deficient and Mixed Valence Perovskites

One of the many useful properties of perovskite type oxides is the relatively high ionic and electronic conductivity exhibited by perovskites with oxygen vacancies and cations capable of adopting mixed valencies respectively[5, 31, 32]. This makes them potentially useful in solid oxide fuel cells (SOFCs), high temperature oxygen separation, electrochemical reactors and oxygen sensors[31, 33]. Of these various applications SOFCs are of particular interest as they provide a method for generating electricity in a cleaner and more efficient manner than conventional power stations that rely on the combustion of coal or hydrocarbons[34, 35]. In a SOFC oxygen is reduced at a cathode and these oxygen anions migrate through the solid electrolyte to the anode where they react with the fuel (see Figure 1.9)[34]. Alternatively a proton conducting electrolyte can be used; in this case the migration of the oxygen anions is replaced by the conduction of protons from the anode to the cathode[33, 34]. This process of reduction at the cathode and oxidation at the anode produces an electrical current that can be harnessed as a source of energy to operate devices. Solid oxide fuel cells have a number of advantages compared to other fuel cell types including high energy conversion efficiency and the ability to use hydrocarbon fuels such as methane or carbon monoxide instead of hydrogen[34]. The high efficiency of conversion of fuel to electricity compared to conventional technology could contribute to decreased CO_2 emission hence reducing the greenhouse effect. SOFCs can be used for both stationary electric power plants and in more mobile electrical generators that could be used, for example, in motor vehicles[36].

A major driving force behind developing new materials for SOFCs is lowering the operating temperature below 800 °C. This would eliminate the need to use expensive alloys for interconnects and current collectors and reduce cracking in components[32]. This requires the development of new cathode and electrolyte materials that have high conductivity at lower temperatures. Cathode materials are required to have good oxygen ion and electronic conductivity while electrolytes require high oxygen anion or proton conductivity with as low electronic conductivity as possible[5, 31, 32]. Compounds with the perovskite structure that are of interest for use as electrolytes include $Sr_xLa_{1-x}GaO_{3-\delta}$ [37] and $BaLn_xCe_{1-x}O_{3-\delta}$[31, 33, 38] because of their high oxygen ion and proton conductivity respectively, while other perovskites such as $Sr_xLa_{1-x}CoO_{3-\delta}$[39-41] and $Sr_xLa_{1-x}MnO_{3-\delta}$[32] are of interest for use as cathodes due to the high electronic and oxygen ion conductivity these compounds exhibit.

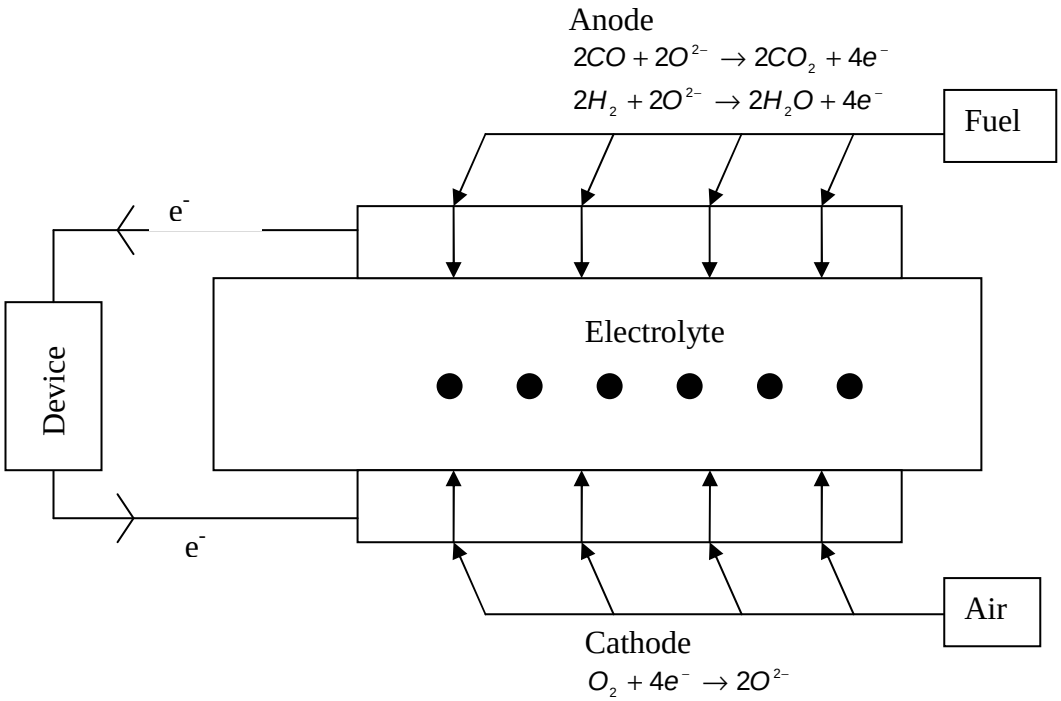

Figure 1.9: Representation of a SOFC where the electrolyte is an oxygen ion conductor and the circles represent oxide anions conducting through the electrolyte.

In general it seems that high oxygen anion or proton conductivity is often associated with a significant level of oxygen vacancies in the structure[31-33]. A higher level of oxygen vacancies provides more vacant oxygen sites for oxygen ion diffusion. In the case of a proton conductor a higher level of oxygen vacancies means that more water

molecules can be accommodated into the structure in the form of hydroxide ions, which introduces more protons into the structure[33]. On the other hand electronic conductivity is often associated with cations that can adopt mixed valencies[5]. Clearly in compounds with a cation that has the potential to have mixed valence states there is a relationship between the level of oxygen vacancies and the amount of the cation oxidised to the higher valence state. If the cation is more readily oxidised doping of the compound with a lower valence ion will lead to cation oxidation rather than creating oxygen vacancies. Conversely doping another compound in the same way that contains a mixed valence cation which has a preference for the lower valence state will result in the formation of more oxygen vacancies. Therefore investigation of the relative stability of valence changes compared to oxygen vacancies is of interest in perovskites that have the potential to be used for their ionic or electronic conductivity.

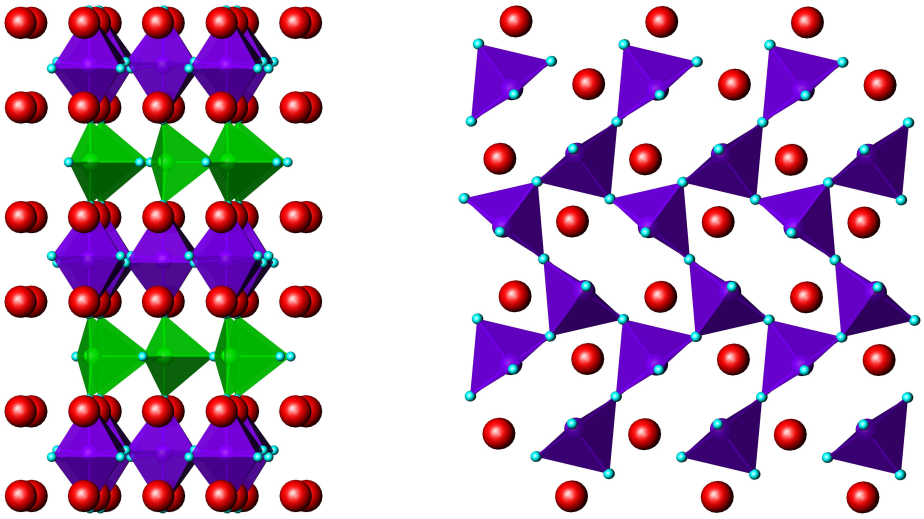

Figure 1.10: Depictions of the oxygen vacancy ordered brownmillerite structure adopted by $Sr_2Fe_2O_5$ (left) and the square pyramidal network of $Ca_2Mn_2O_5$ (right).

In perovskites with high levels of oxygen vacancies the strong electrostatic forces between vacancies tend to lead to the formation of ordered phases such as the brownmillerite structure adopted by $Sr_2Fe_2O_5$ or the $Ca_2Mn_2O_5$ structure (see Figure 1.10)[1, 5]. In ordered structures there is a large energy cost for the oxygen anions moving from the occupied site to the empty site because of the chemical differences between these environments. This reduces the conductivity of such materials[5]. Partial ordering of oxygen vacancies in perovskite structures with octahedral tilting is, however, of interest due to the potential influence this has on the pathway of oxygen

ion conduction and the potential for having some anisotropy in the ionic conductivity along various axes of the crystal structure[42]. The pathway of oxygen ion conduction in some perovskites has recently been examined by Yashima *et al.*[43, 44] who found that oxygen anions in perovskites move in an arced fashion rather than in a straight line between oxygen anion sites. Furthermore it was found that in the case of the A-site vacancy layered perovskite $La_{0.64}Ti_{0.92}Nb_{0.08}O_{2.99}$ the conductivity pathway appears to be two dimensional in the plane perpendicular to the layered axis (see Figure 1.11 for the crystal structure of this compound). This indicates the potential for anisotropic conductivity in materials with partially ordered vacancies.

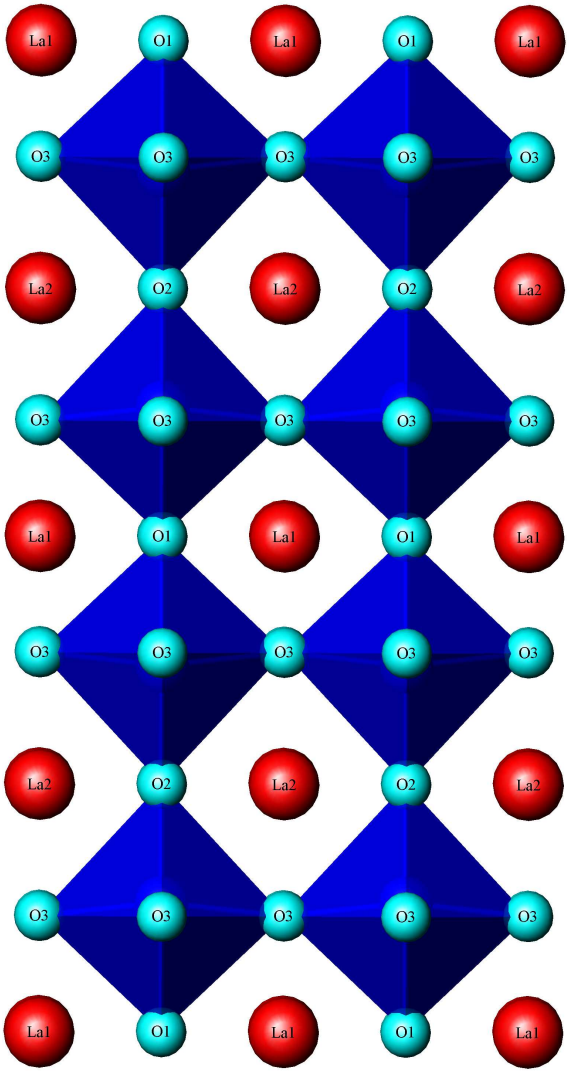

Figure 1.11: High temperature crystal structure of $La_{0.64}Ti_{0.92}Nb_{0.08}O_{2.99}$. The La1 site is fully occupied while La2 is a partially occupied site. Yashima *et al.*[43] suggest

that oxygen ions occupying the O3 site are the most mobile anions and diffuse in the planes occupied by O3 atoms in a curved fashion between adjacent O3 sites.

Partial oxygen vacancy ordering is possible in tilted perovskites since many of these structures have two or more crystallographically distinct anion sites. The oxygen vacancies may concentrate onto one site leaving it partially filled while the other sites are fully occupied. Neutron diffraction studies of $BaCe_{1-x}Ln_xO_{3-\delta}$, $La_{1-x}Sr_xGaO_{3-\delta}$ and $Ln_{1-x}Sr_xCoO_{3-\delta}$ indicate that the oxygen vacancies tend to concentrate exclusively on equatorial sites of the octahedra[40, 42, 45, 46]. On the other hand in $La_{1-x}Sr_xGa_{1-x}Mg_xO_{3-\delta}$ some structures have been suggested to have rhombohedral or cubic symmetry that have only one oxygen atom crystallographic site thus requiring all the oxygen atoms to be uniformly distributed throughout the structure[42, 47]. This suggests that when oxygen vacancies occur in tilted perovskites that have distinctly different oxygen sites they preferentially concentrate on one site, but in structures that only have one oxygen environment the formation of oxygen vacancies does not result in the formation of a structure with multiple oxygen sites.

The structures of double perovskites with significant levels of oxygen vacancies have not been well studied. Of the known oxygen deficient double perovskites, $Ba_2YSnO_{5.5}$ is one of the most promising for applications requiring ionic conductivity such as SOFCs[48]. $Ba_2YSnO_{5.5}$, a member of the $Ba_2LnSnO_{6-\delta}$ $(0 \leq \delta \leq 0.5)$ series of compounds[48-51], has amongst the highest levels of proton conductivity below 300 °C known to date and also exhibits oxide conductivity at higher temperatures. The structures of $Ba_2LnSnO_{6-\delta}$ compounds have been described as cubic; they therefore belong to space group $Fm\bar{3}m$ and have no ordering of the oxygen vacancies. The reported studies however have been carried out using conventional powder X-ray diffraction so further analysis using high resolution synchrotron X-ray and neutron diffraction is required to confirm this symmetry. In particular neutron diffraction will allow identification of the position of oxygen vacancies in the structure and potentially the site the proton occupies in the hydrated material.

Although the $Ba_2LnSnO_{6-\delta}$ oxides have high chemical stability, upon reduction the structure collapses and a brownmillerite structure forms, as can be seen in the case of

$Ba_2YSnO_{5.5}$[48]. This is a problem for the potential application of these compounds. Murugaraj *et al*.[48] proposed that this is caused by the high level of oxygen deficiency in this structure. One possible way to increase the stability of these structures under reducing conditions would be to reduce the level of oxygen deficiency by doping the Sn^{4+} site with a pentavalent cation of a similar size such as Sb^{5+} and Nb^{5+} (cf. 0.69, 0.64 and 0.60 Å for Sn^{4+}, Nb^{5+} and Sb^{5+} respectively[52]) that are known to form double perovskite structures of the type $Ba_2LnB'O_6$ (B' = Nb^{5+} or Sb^{5+})[28, 53, 54]. Doping with Nb^{5+} and Sb^{5+} will allow control of both the level of oxygen deficiency and the symmetry of the structure of these compounds. The later would be related to the location of the oxygen vacancies in these oxygen deficient perovskites. Additionally using either Pr^{3+} or Tb^{3+} as the lanthanide will allow the examination of the relative stability of oxygen vacancies in $Ba_2LnSn_xB'_{1-x}O_{6-\delta}$ (where B' = Sb^{5+} or Nb^{5+}). This is because these lanthanides can adopt a tetravalent state hence reducing or eliminating oxygen vacancies from this structure if the change in valence state is preferable to a high level of oxygen deficiency. How such a change in valency affects the structure adopted by a perovskite and whether any valence state change occurs gradually or discontinuously is of itself fundamentally interesting. Structural characterisation of compounds in the $Ba_2LnSn_xB'O_{6-\delta}$ family have been carried out as part of this work and are presented in Chapters 5 and 6.

1.6 References

[1] R.H. Mitchell, *Perovskites Modern and Ancient*, Almaz Press, Ontario, 2002.

[2] M.T. Anderson, K.B. Greenwood, G.A. Taylor, K.R. Poeppelmeier, Prog. Solid State Chem. 22 (1993) 197-233.

[3] O.P. Kulik, Powder Metall. Met. Ceram. 38 (1999) 93-101.

[4] P.A. Cox, *Transition Metal Oxides: An Introduction to Their Electronic Structure and Properties*, Clarendon Press, Oxford, 1992.

[5] J.B. Goodenough, Rep. Prog. Phys. 67 (2004) 1915-1993.

[6] H.D. Megaw, C.N.W. Darlington, Acta Cryst. A 32 (1975) 161-173.

[7] V.M. Goldschmidt, Naturwissenschaften 14 (1926) 477-485.

[8] A.M. Glazer, Acta Cryst. B 28 (1972) 3384-3392.

[9] C.J. Howard, H.T. Stokes, Acta Cryst. B 54 (1998) 782-789.

[10] M.T. Anderson, K.R. Poeppelmeier, Chem. Mater. 3 (1991) 476-482.

[11] C.J. Howard, B.J. Kennedy, P.M. Woodward, Acta Cryst. B 59 (2003) 463-471.

[12] C.A. Randall, A.S. Bhalla, T.R. Shrout, L.E. Cross, J. Mater. Res. 5 (1990) 829-834.

[13] P.M. Woodward, Acta Cryst. B 53 (1997) 44-66.

[14] A.F. Wells, *Structural Inorganic Chemistry*, Clarendon Press, Oxford, 1991.

[15] I.D. Brown, D. Altermatt, Acta Cryst. B 41 (1985) 244-247.

[16] T. Wolfram, S. Ellialtioglu, *Electronic and Optical Properties of d-Band Perovskites*, Cambridge University Press, Cambridge, 2006.

[17] P.M. Woodward, Acta Cryst. B 53 (1997) 32-43.

[18] M.W. Lufaso, P.M. Woodward, Acta Cryst. B 57 (2001) 725-738.

[19] L. Pauling, J. Am. Chem. Soc. 51 (1929) 1010-1026.

[20] R. Diehl, G. Brandt, Mater. Res. Bull. 10 (1975) 85-90.

[21] G. Bergerhoff, I.D. Brown, in: F.H. Allen, G. Bergerhoff, R. Sievers (Ed.), *Crystallographic Databases*, International Union of Crystallography, Chester, 1987, p. 77-95.

[22] M.W. Lufaso, P.W. Barnes, P.M. Woodward, Acta Cryst. B 62 (2006) 397-410.

[23] S.-H. Byeon, S.-S. Lee, J.B. Parise, P.M. Woodward, N.H. Hur, Chem. Mater. 17 (2005) 3552-3557.

[24] S.-H. Byeon, M.W. Lufaso, J.B. Parise, P.M. Woodward, T. Hansen, Chem. Mater. 15 (2003) 3798-3804.
[25] W.T. Fu, D.J.W. IJdo, J. Solid State Chem. 179 (2006) 1022-1028.
[26] W.T. Fu, D.J.W. IJdo, Solid State Commun. 136 (2005) 456-461.
[27] W.T. Fu, D.J.W. IJdo, J. Alloys Compd. 394 (2005) L5-8.
[28] W.T. Fu, D.J.W. IJdo, J. Solid State Chem. 178 (2005) 2363-2367.
[29] E.J. Cussen, D.R. Lynham, J. Rogers, Chem. Mater. 18 (2006) 2855-2866.
[30] W.T.A. Harrison, K.P. Reis, A.J. Jacobson, L.F. Schneemeyer, J.V. Waszczak, Chem. Mater. 7 (1995) 2161-2167.
[31] V.V. Kharton, F.M.B. Marques, A. Atkinson, Solid State Ionics 174 (2004) 135-149.
[32] S.J. Skinner, Int. J. Inorg. Mater. 3 (2001) 113-121.
[33] K.D. Kreuer, Solid State Ionics 97 (1997) 1-15.
[34] O. Yamamoto, Electrochim. Acta 45 (2000) 2423-2435.
[35] F. Tietz, H.-P. Buchkremer, D. Stöver, Solid State Ionics 152-153 (2002) 373-381.
[36] N.Q. Minh, Solid State Ionics 174 (2004) 271-277.
[37] T. Ishihara, H. Matsuda, Y. Takita, J. Am. Chem. Soc. 116 (1994) 3801-3803.
[38] H. Iwahara, T. Mori, T. Hibino, Solid State Ionics 79 (1995) 177-182.
[39] H.Y. Tu, Y. Takeda, N. Imanishi, O. Yamamoto, Solid State Ionics 100 (1997) 283-288.
[40] M. James, D. Cassidy, D.J. Goossens, R.L. Withers, J. Solid State Chem. 177 (2004) 1886-1895.
[41] V.V. Kharton, A.P. Viskup, E.N. Naumovich, N.M. Lapchuk, Solid State Ionics 104 (1997) 67-78.
[42] M. Kajitani, M. Matsuda, A. Hoshikawa, S. Harjo, T. Kamiyama, T. Ishigaki, F. Izumi, M. Miyake, Chem. Mater. 17 (2005) 4235-4243.
[43] R. Ali, M. Yashima, F. Izumi, Chem. Mater. 19 (2007) 3260-3264.
[44] M. Yashima, K. Nomura, H. Kageyama, Y. Miyazaki, N. Chitose, K. Adachi, Chem. Phys. Lett. 380 (2003) 391-396.
[45] R.L. Withers, M. James, D.J. Goossens, J. Solid State Chem. 174 (2003) 198-208.
[46] K.S. Knight, Solid State Ionics 145 (2001) 275-294.

[47] M. Kajitani, M. Matsuda, A. Hoshikawa, K.-i. Oikawa, S. Torii, T. Kamiyama, F. Izumi, M. Miyake, Chem. Mater. 15 (2003) 3468-3473.
[48] P. Murugaraj, K.D. Kreuer, T. He, T. Schober, J. Maier, Solid State Ionics 98 (1997) 1-6.
[49] J. James, O.B.S. Kumar, S.S. Kumar, P.P. Rao, K.V.O. Nair, Mater. Lett. 57 (2003) 3641-3647.
[50] J. Koshy, K.S. Kumar, J. Kurian, Y.P. Yadava, A.D. Damodaran, J. Am. Ceram. Soc. 78 (1995) 3088-3092.
[51] J. Koshy, K.S. Kumar, J. Kurian, Y.P. Yadava, A.D. Damodaran, Physica C 234 (1994) 211-218.
[52] R.D. Shannon, Acta Cryst. A 32 (1976) 751-767.
[53] K. Henmi, Y. Hinatsu, N.M. Masaki, J. Solid State Chem. 148 (1999) 353-360.
[54] P. García Casado, A. Mendiola, I. Rasines, Z. Anorg. Allg. Chem. 510 (1984) 194-198.